Catalysis Today 155 (2010) 51–58

Contents lists available at ScienceDirect

Catalysis Today

journal homepage: www.elsevier.com/locate/cattod

Methane oxidation over palladium-washcoated foils in the presence of sulphur dioxide

G.L. Rickett *, V. Dupont, M.V. Twigg [1]

ERRI, SPEME, The University of Leeds, Leeds, LS2 9JT, UK

ARTICLE INFO

Article history:
Available online 1 May 2009

Keywords:
Kinetics
Catalytic
Methane
Sulphur and palladium

ABSTRACT

The catalytic oxidation of methane in the presence and absence of SO_2 was investigated on palladium catalysts supported on Al_2O_3 and CeO_2/Al_2O_3 washcoats. The washcoats adhered onto thin stainless steel foils and were investigated under fuel-lean conditions in a stagnation point flow reactor (SPFR). Both palladium-loaded washcoats exhibited hysteresis in the conversion versus temperature profile during heating and cooling. This was attributed to the change in oxidation state of palladium between PdO and Pd. The presence of CeO_2 stabilised PdO, reducing the extent of the conversion discontinuities caused by the PdO ↔ Pd transitions during heating and cooling. However, the $Pd/CeO_2/Al_2O_3$ catalyst had a lower activity for methane oxidation. The presence of SO_2 in the feed deactivated both catalysts, but unexpected higher conversions following exposure to SO_2 reflected a promotional effect in the thermal decomposition region of PdO. Exposure to 30 ppm SO_2 in the lean methane feed stream eliminated the stabilising effects that CeO_2 had on conversion during the PdO–Pd transition. Frequency factors and activation energies were calculated for a single step reaction mechanism using a power law kinetic model. The numerical code SPIN successfully modelled the conversion curves using the derived kinetic data, providing a means of kinetic validation. The activation energies in absence of SO_2 were 44 ± 1 kJ mol^{-1} and 58 ± 4 kJ mol^{-1} for the 3 wt.% Pd/Al_2O_3 and the 3 wt.% Pd/12 wt.% CeO_2/γ–Al_2O_3 catalyst respectively, one of the lowest reported in the literature. The aged catalysts also exhibited relatively low activation energies (49–84 kJ mol^{-1}).

1. Introduction

The durability and poisoning of combustion catalysts are factors which need to be taken into account during catalyst selection. The present study investigates the effects of SO_2 on methane oxidation over palladium supported catalysts. Methane is in abundance from fossil and renewable biological sources, it is difficult to burn and has high H/C ratio. The latter means more energy is produced per unit mass of CO_2 generated. This coupled with high efficiencies of modern natural gas fired combustors make methane an important fuel of the future.

Sulphur species are added as odorants to natural gas. Sewage gases, gasification gases from coal and biomass also contain high concentrations of H_2S and other sulphur compounds that are readily oxidized to SO_2 at moderate temperatures. Under lean conditions palladium oxide catalysts are the most active catalyst for methane oxidation. In the present study the catalyst was washcoated onto thin (57 μm) stainless steel foil, bearing similarities with the walls of a honeycomb monolith catalyst. This provides a closer approximation to many catalytic combustors conditions than previously used powders.

2. Experimental

2.1. Reactor configuration

The stagnation point flow reactor (SPFR) was used in the present investigation and Fig. 1 shows the experimental configuration. The reactants were premixed prior to entering the reactor. The feed streams of CH_4/air/N_2 were regulated by three mass flow controllers. A programmable syringe pump provided the SO_2 content of the feed streams. The air to fuel ratio was changed while keeping the total flow rate and nitrogen mol fraction constant at 451.2 cm^3 min^{-1} STP and 0.88 respectively.

The stoichiometry is defined by the parameter $\alpha = \dot{V}_{CH_4}/(\dot{V}_{CH_4} + \dot{V}_{O_2})$ where $\dot{V}_i$ is the volumetric flow rate of the gas concerned. Values lower than 1/3 were used in the present study, corresponding to fuel-lean operation. The relationship between α and the equivalence ratio ϕ for methane combustion is $\phi = 9.52/(1 + 79/21)(1/\alpha - 1)$. The reactants entered the reactor via the injector which had an internal diameter of 23.5 mm. The injector housed a series of wire meshes to

* Corresponding author. Tel.: +44 0 113 343 2353; fax: +44 0 113 246 7310.
E-mail address: g.l.rickett@leeds.ac.uk (G.L. Rickett).
[1] Johnson Matthey Plc., Orchard Road, Royston, SG8 5HE, UK.

0920-5861/$ – see front matter © 2009 Elsevier B.V. All rights reserved.
doi:10.1016/j.cattod.2009.03.013

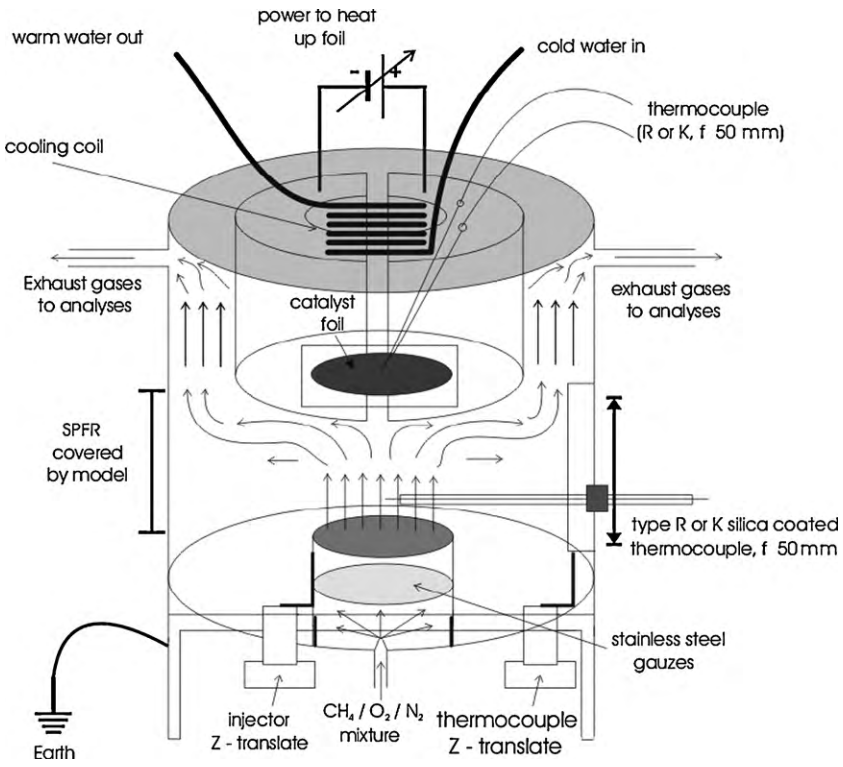

Fig. 1. Schematic of the experimental setup of the stagnation point flow reactor.

achieve uniform flow. The separation distance between injector and catalyst was fixed at 3 mm, yielding a distance to diameter ratio lower than 0.13, and a good practical approximation to the 'infinite' diameter assumptions of the theoretical stagnation point flow configuration model. The washcoated foils were evenly electrically heated in a disc shape with the same diameter as the injector, by semicircular shaped electrodes. A type K thermocouple was spot welded at the back and center of the foil, with standard 50 μm diameter wires. This thermocouple controlled the temperature of the foil using a closed loop PID circuit. In some of the experiments three thermocouples were present: at the center, 3.5 mm and 7 mm off-center, aligned with and on either side of the foil center. Measurements carried in the absence of methane in the flow indicated lower temperatures by typically 16 K and 25 K for the 3.5 mm and the 7 mm off-center positions, but these reduced to 5 K and 10 K respectively when methane was present in the bulk gas mixture due to the exothermicity of the combustion reaction at the surface. A surface weighted averaged temperature was calculated with the three temperatures and the value obtained was close to the measured 3.5 mm off-center temperature. Kinetic model tests were carried out by using as input temperature the center temperature minus 5 K, associated an absolute 5 K uncertainty. The activation energy and pre-exponential factors obtained were not statistically different to those derived using the center foil temperature as input, therefore the center-foil temperature was used henceforth as the basis for the kinetic model input. Temperature gradients of less than 0.06 K over the washcoat thickness were calculated, allowing the measured temperature at the back of the foil to accurately represent the temperature at the bulk gas-washcoat interface. More information on the experimental setup can be found in [1].

2.2. Preparation and temperature cycles

The experiments were performed over 3 wt.% Pd/γ-Al_2O_3 and 3 wt.% Pd/12 wt.% CeO_2/γ-Al_2O_3 catalysts. The catalysts were washcoated with an average thickness of 9 μm onto stainless steel foil 57 ± 2 μm thick, by Johnson Matthey, to approximate the conditions in a honeycomb monolithic catalyst. Slurries of alumina and alumina–ceria were used, that were impregnated with Pd (II) nitrate after washcoating. The catalysts had nitrogen BET areas of 117 $m^2\ g^{-1}$ and 135 $m^2\ g^{-1}$ for Al_2O_3 and Al_2O_3/CeO_2 respectively. The loadings of the washcoats were 0.59 ± 0.2 mg cm^{-2} and 0.80 ± 0.4 mg cm^{-2} respectively. The catalysts were pretreated prior to testing by exposing them to air with a flow rate of 1000 $cm^3\ min^{-1}$ STP for 1 h at 773 K. Experimental cycles were then performed where the temperature of the catalyst (T_{s-g}) was slowly increased and then decreased incrementally in steps. At each temperature step the reactor was allowed to reach steady state before taking readings. After each temperature cycle the catalyst was prepared for the next run by flowing air through the reactor as described above, but this time for 30 min. The experiments were carried out in order of increasing methane concentration.

2.3. Analyses of combustion products

Combustion product analyses were carried out using two on-line analysers connected in parallel. The SO_2 concentration was measured on a wet basis using a UV (285 nm) absorption analyser with a heated line (ABB Limas 11). The oxygen concentration was measured on a dry basis (±500 ppm) by a Servomex paramagnetic analyzer preceded by an ice bath and a silica gel trap. It was shown via infrared absorption that no measurable amount of CO was generated in any of the cycles. This enabled the methane conversion for a given catalyst temperature to be calculated from an O_2 balance.

3. Modelling

3.1. Code SPIN

The code SPIN was used to model the reactor and to provide validation of the derived kinetic parameters. A detailed description of the model is given in the user manual [2]. The global reaction

rate for methane oxidation can be expressed by a power law model and the Arrhenius expression ($k = A\exp(-E/RT)$), where A and E are the frequency factor and activation energy of the reaction respectively. The concentrations of reactants at the solid catalyst–gas interface can be substituted out of the rate expression for gas fraction using the ideal gas law to give:

$$k = \frac{\dot{\omega}_{i,\mathrm{HET}}}{X^{a}_{\mathrm{CH_4,s-g}} \times X^{b}_{\mathrm{O_2,s-g}} (P/RT_{\mathrm{s-g}})^{a+b}} \quad (1)$$

$$\ln k = \ln A - \frac{E}{RT_{\mathrm{s-g}}} \quad (2)$$

where $T_{\mathrm{s-g}}$ is the temperature at the solid–gas interface of the catalyst. The terms $X_{\mathrm{CH_4,s-g}}$ and $X_{\mathrm{O_2,s-g}}$ are the molar gas fractions of methane and oxygen at the solid–gas (s–g) interface respectively, these can be expressed as a linear function of the conversion as explained in the methodology outlined in [3]. We have shown in [3] that these linear functions are independent of the rate constants. One can therefore determine the constants of the ($X_{i,\mathrm{s-g}}$ versus conversion) linear function by running SPIN at a low and a high ($T_{\mathrm{s-g}}$, conversion) pair with assumed values of E and A. The universal gas constant and reactor pressure is given by R and P. Eq. (2) can be used to derive the kinetic parameters by performing a linear regression in the absence of gas phase combustion. In a plot of $\ln k$ against $1/T_{\mathrm{s-g}}$, the intercept is $\ln A$ and the gradient ($-E/R$). Once the kinetic rate had been derived, an analysis of the effectiveness factor was carried out to determine the range of data leading to kinetic control [4] and all datapoints yielding an effectiveness factor of less than 0.9 were rejected from the fit, the results of which are illustrated in the end of the results section. The effectiveness factor was calculated using the procedure outlined in [3]. Desorption isotherms were used to calculate the pore size distribution using Kelvin's equation [5]. The t-method [5], which allows the determination of total micropores volume, was applied to the desorption isotherm data. The resulting plot of volume of N_2 adsorbed versus t revealed an intercept near zero, indicating that there was a negligible microporous structure.

4. Results

4.1. Methane oxidation

The catalytic oxidation of methane over fresh 3 wt.% Pd/γ-A_2O_3 was investigated first. Fig. 2(a) shows the methane conversion curves for different values of α when the nitrogen concentration was kept constant with increasing temperature. Fig. 2(a) also shows the conversion predicted by SPIN using the derived kinetic values of E and A as inputs. Values of E and A for selected experiments are also given in Table 1 (shown at the end of the results section). Table 1 also lists the number of points used for the linear fit, the value of the correlation coefficient r (between 0.97 and 0.99), the range of temperatures and conversions used for the fit, and the range of effectiveness factors (η) calculated for each fit. It can be seen the fits were carried out from the lowest conversion and temperature range, and that η was always above 0.9, indicating the conditions were away from diffusion control.

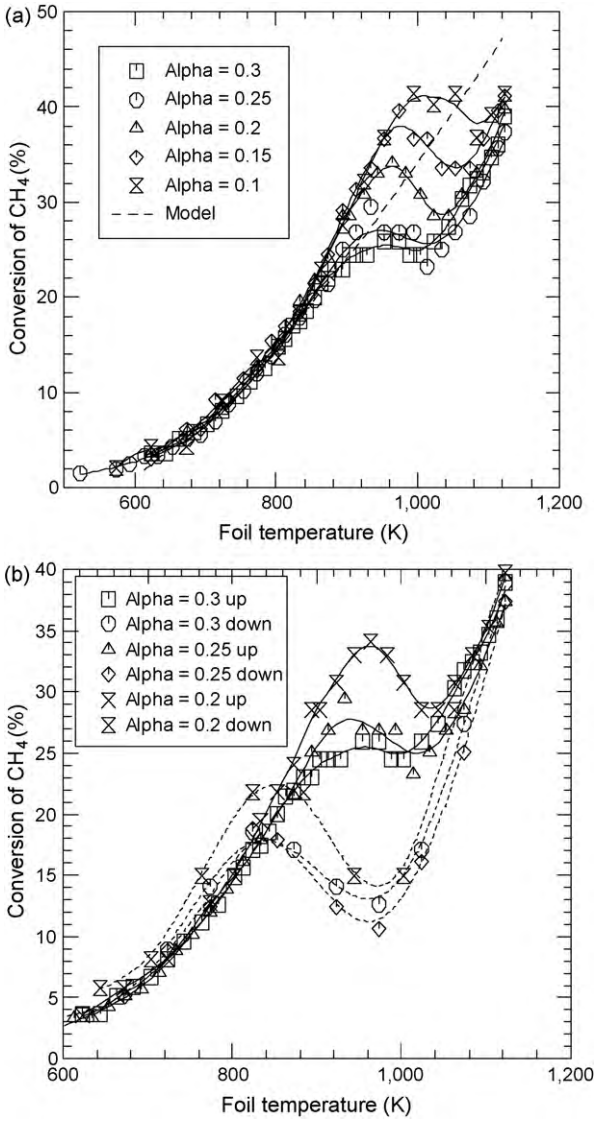

Fig. 2. Methane conversion cycles over 3 wt.% Pd/γ-Al_2O_3 for different values of α under lean conditions with N_2 constant at $X_{N_2} = 0.88$. (a) Increasing temperature steps for α values of 0.1–0.3 following experimental procedure outlined in 2.2. (b) Full temperature cycles for three selected values of α, labeled up' and 'down' for increasing and decreasing temperature respectively. For a same α, and 'up' labeled curve followed by 'down' represent a full cycle experiment.

Table 1
Kinetic parameters of A and E derived from the linear fits shown in Fig. 8, r is the linear correlation coefficient, Pts is the number of points used, η is the effectiveness factor range, and conversion is the methane conversion range used for the fit.

Fit	Catalyst	α	A (cm s^{-1})	E (kJ mol^{-1})	Pts	r	T (K)	η (effectiveness factor)	Conversion (%)
	Fresh								
□	Pd/Al_2O_3	0.25	$(5.9 \pm 0.8) \times 10^2$	44 ± 1	13	0.99	573–813	0.99–0.91	2.0–16.1
⧖	$Pd/CeO_2/Al_2O_3$	0.25	$(1.0 \pm 0.5) \times 10^3$	58 ± 4	5	0.97	723–873	0.98–0.90	1.5–7.5
	With SO_2								
○	Pd/Al_2O_3	0.20	$(6.0 \pm 2) \times 10^4$	81 ± 2	8	0.99	723–898	0.99–0.90	2.3–19.4
↑	$Pd/CeO_2/Al_2O_3$	0.20	$(2.2 \pm 0.9) \times 10^4$	84 ± 3	7	0.99	773–923	0.98–0.9	1.2–6.9
	With SO_2								
△	Pd/Al_2O_3	0.25	$(2.1 \pm 0.6) \times 10^4$	73 ± 2	11	0.98	673–873	0.99–0.91	1.4–16.0
⧖	$Pd/CeO_2/Al_2O_3$	0.25	$(3.7 \pm 1) \times 10^2$	49 ± 2	9	0.99	723–843	0.97–0.9	2.4–5.1

Fig. 2(b) shows conversions for increasing and decreasing temperature cycles for different values of α.

The reactant orders for methane and oxygen were assumed to be one and zero respectively, due to the high excess air (e.g. [6]). This is corroborated by the fact that at low temperatures the conversion curves for the different values of α are superimposable and by the excellent fit given by the model upto 900 K. The data in Fig. 2(a) for α of 0.25 were used to estimate the parameters under these conditions: an activation energy of 44 kJ mol^{-1} and a pre-exponential factor of 5.9×10^2 cm s^{-1} (listed in Table 1) were obtained with a correlation coefficient exceeded 0.99 using the 13 points, indicating an excellent fit. There are many different values of E and A in the literature for the same reaction, with E values ranging from 56.1 kJ mol^{-1} to 137 kJ mol^{-1} for Pd supported catalysts, therefore the value of 44 kJ mol^{-1} would appear as the lowest reported and is attributed to the use of the thin washcoated foil and the SPFR configuration to derive kinetics. However the lower activation energy found for the present setup was counter-intuitive. In previous work [3], a comparison between activation energies obtained for Pt-Al_2O_3 powder catalysts and Pt-containing washcoats using the same catalyst formulation but supported on steel foil revealed the foils had a significantly higher activation energy and lower activity. The opposite was found here for Pd washcoats on steel foil. It may be that the differences in chemistry between Pd- and Pt-catalysed methane oxidation yield opposite effects with thinly washcoated catalysts. This result stresses the importance that the catalyst form has on derived kinetics and suggests caution when using powder-derived kinetics in thin washcoat models. An example of high E for the Pd catalyst is 130.4 kJ mol^{-1} with A of 2.1×10^8 s^{-1} under lean condition for 5 wt.% Pd/Al_2O_3 with the same reactant orders [6]. However it is notoriously difficult to make comparisons between the published data where differences in catalysts, and in assumed kinetic models exist [4].

A drop in conversion, which was followed by an increase, henceforth called a 'discontinuity' was observed above 1000 K. This was attributed to the change in oxidation state of palladium at high temperature. This agreed with the decomposition temperature of PdO found using thermodynamic data [7]. The predicted decomposition temperatures were as follows: 1000 K, 1006 K, 1015 K, 1019 K and 1020 K for α of 0.3, 0.25, 0.2, 0.15 and 0.1 respectively. The method of calculating the decomposition

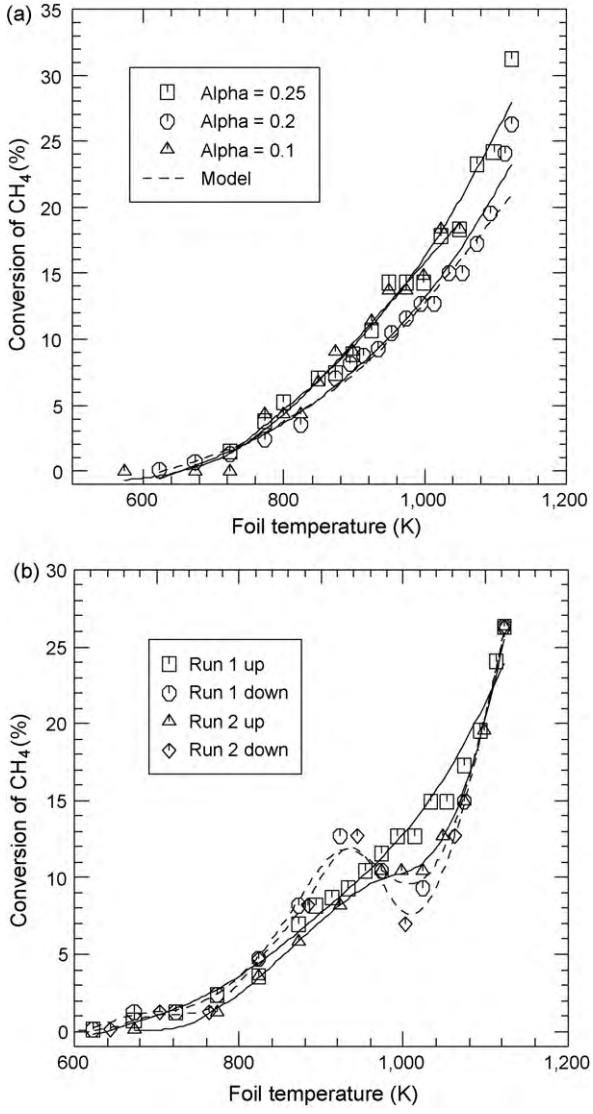

Fig. 3. Methane conversion cycles over 3 wt.% Pd/12 wt.% CeO_2/γ-Al_2O_3 for different values of α under lean conditions with N_2 constant at $X_{N_2} = 0.88$. (a) Increasing temperature steps for α of 0.1 to 0.25. (b) Full temperature cycle for α of 0.2 (labeled 'run up' and 'run down' for increasing and decreasing temperature respectively).

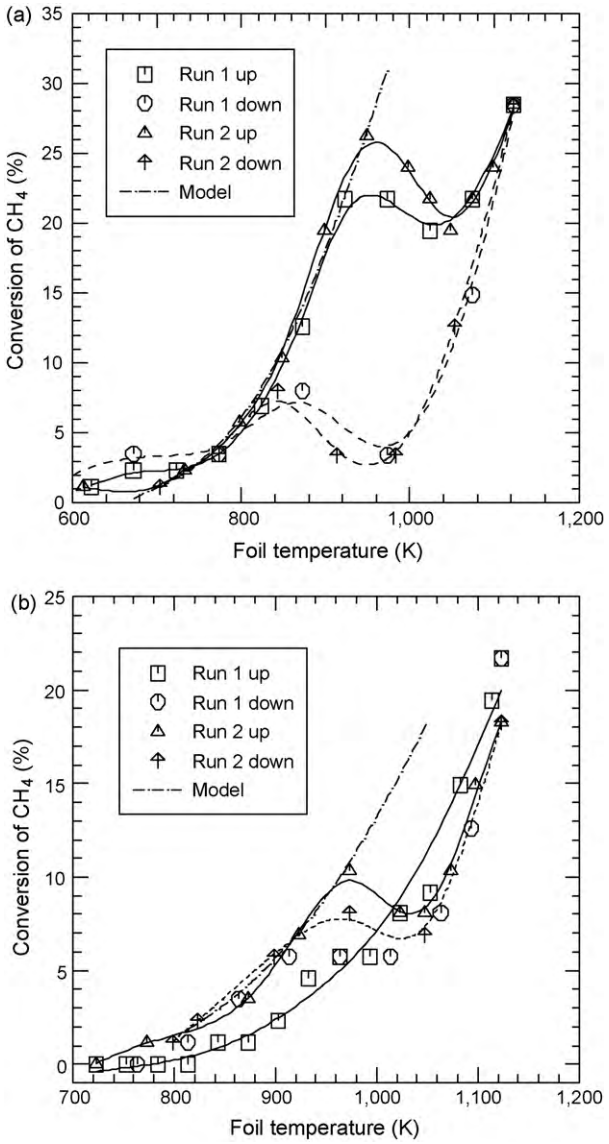

Fig. 4. Methane conversion for two repeated cycles in the presence of 30 ppm SO_2 in the feed stream, under lean conditions α = 0.2 and $X_{N_2} = 0.88$. (a) 3 wt.% Pd/γ-Al_2O_3. (b) 3 wt.% Pd/12 wt.% CeO_2/γ-Al_2O_3, labels 'up' and 'down' as for Fig. 3b.

temperature from thermodynamic data is given in [4]. The increase in methane conversion after the decomposition of PdO to Pd was attributed to the catalytic activity of metallic Pd, which offers a higher activation energy than PdO. The Pd then reverts to PdO in the decreasing temperature curve, exhibiting lower conversion than during the PdO–Pd conversion, seen as a negative hysteresis in Fig. 2b. This is consistent with previous work [8], which found that in the transition metal-oxide, Pd was less active than PdO. Here, the hysteresis covers the temperature region (850–1020 K). This also is in agreement with earlier work [9] which reported a detailed investigation into the reduction and re-oxidation of Pd supported on γ-Al_2O_3 powdered catalyst. Other work [10] also showed the same negative hysteresis on 4 wt.% PdO/Al_2O_3. They attributed this to the formation of an oxygen-Pd species given as PdO_x/Pd. Farrauto et al. [10] found the observed increased oxygen adsorption exceeded a monolayer coverage. This indicated oxygen penetrated below the surface of the Pd particles. This was in agreement with Mowery and McCormick [11] who presented a reaction mechanism involving diffusion of oxide ions to the core of the Pd crystallites and also with oxygen penetration studies [12]. It was also observed that decreasing the value of α led to an increase in the temperature at which PdO decomposed. This was due to the higher oxygen concentration of lower values of α and can be explained thermodynamically as discussed above. When the catalyst temperature was decreased (which is represented by the broken lines in Figs. 2–5), lower conversion was obtained than when increasing the temperature for the first part of the cycle. However, when the catalyst temperature was reduced beyond the decomposition temperature, the conversion was restored to its original value. This was therefore attributed to the re-oxidation of metallic Pd back to PdO.

The test cycles used for Pd/Al_2O_3 were then performed on the 3 wt.% Pd/12 wt.% CeO_2/γ-Al_2O_3 catalyst. With CeO_2 present, PdO was more stable, but the fresh catalyst activity was less. These effects are shown in Fig. 3(a and b) where no clear discontinuity due to thermal decomposition of PdO was observed, indicating the presence of CeO_2 stabilising PdO.

TEM was used to estimate the size of the Pd or PdO crystallites and hence the surface areas. Metal Pd/PdO particles sizes were measured for 63 particles on fresh Al_2O_3 and 36 particles on fresh CeO_2/Al_2O_3 washcoats. The results revealed the fresh CeO_2 washcoated catalyst had Pd or PdO crystallites approximately 10% greater in size than those of the fresh catalyst without CeO_2, explaining why the presence of CeO_2 in the support somewhat lowers catalyst activity. The first two rows of Table 1 give the kinetic parameters for both the fresh catalysts. It can be seen that adding CeO_2 to the support doubles the pre-exponential factor whereas the activation energy increased from 44 kJ mol^{-1} to 58 kJ mol^{-1}. The temperature used for the linear fit is also shifted from 573–813 K for the catalyst without ceria, to the higher 723–873 K when ceria-doped.

When all of the temperature cycles were plotted for the ceria-doped catalyst at various values of α (Fig. 3(b)), the decreasing temperature conversion curves for the two runs exhibited a trough followed by a peak, henceforth called a 'discontinuity' around the increasing temperature curve in the 850–1050 K. This phenomenon was significantly smaller than that shown in Fig. 2(b) for the catalyst without CeO_2. A similar effect was shown in previous work [13] on 3 wt.% Pd/10%CeO_2/Al_2O_3 in powder form and was attributed to ceria stabilizing PdO decomposition. This often observed phenomenon is accompanied with a higher extent of Pd oxidation, resulting in a smaller Pd-PdO hysteresis. This work concluded that the oxidation of Pd upon cooling occurred in two steps: at high temperature for Pd crystallites in contact with ceria (due to ceria's redox properties), and at low temperature for oxidation of the Pd particles in contact with Al_2O_3 only.

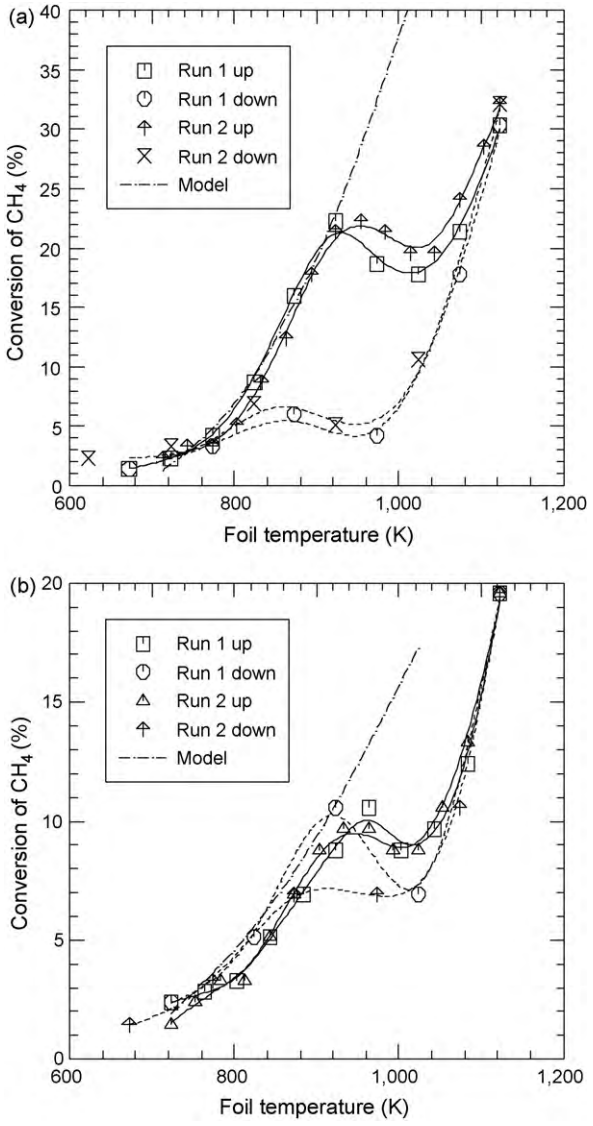

Fig. 5. Methane conversion for two repeated cycles when the catalysts were exposed to 30 ppm SO_2 in the feed stream, under lean conditions $\alpha = 0.25$ and $X_{N_2} = 0.88$. 'Up' and 'Down' labels as for Fig. 3b. (a) 3 wt.% Pd/γ-Al_2O_3. (b) 3 wt.% Pd/12 wt.% CeO_2/γ-Al_2O_3.

Consequently, the presence of a smaller hysteresis in the temperature conversion curves in Fig. 3(b) located at higher temperatures would indicate that the Pd crystallites were in intimate contact with the promoter ceria. So no discontinuity in conversion is observed with increasing temperature.

After the methane oxidation experiments both catalysts (with and without CeO_2) were subjected to low levels of SO_2 during methane oxidation cycles. Both feed streams contained low levels of SO_2 before the start of each cycle from when the catalyst was at room temperature. The concentrations of SO_2 were kept constant at 30 ppm throughout each cycle. At the end of each cycle, stopping the SO_2 feed was done at room temperature, leaving the other reactants flowing through the reactor to flush out remaining SO_2. The first value of α used in the presence of SO_2 was 0.2 and the methane conversion curves for both catalysts are shown in Fig. 4(a). When comparing the methane conversion curves in the absence and presence of SO_2, it can be concluded that the presence of SO_2 in the feed stream deactivates the catalyst, much as would be expected. This deactivation is attributed to the formation of PdO–SO_x sites and is known to be inhibited by

sulphating supports such as Al_2O_3 due to shunting of SO_3 to the support [14].

The same effect was found for the CeO_2 containing catalyst. Fig. 4(b) shows the methane conversion curves for two complete temperature cycles. One interesting observation is that the increasing temperature conversion curve shows a similar small discontinuity (attributable to the decomposition of PdO) to that observed without CeO_2. However, there was no significant hysteresis between the increasing and decreasing temperature conversion curves such as that observed for the ceria-free catalyst. After the first cycles with SO_2, the catalysts were pretreated as described in Section 2.2 and two methane oxidation cycles in the absence of SO_2 were carried out with the same value of α as with SO_2. The aim of this was to determine how much each doping cycle permanently deactivated the catalysts.

After investigating the effect of SO_2 at the α value of 0.2 the catalysts then underwent the same cycles with SO_2 with the α value of 0.25.

Fig. 5(a and b) shows the two methane oxidation cycles for each of the catalysts tested. Again the presence of SO_2 had the effect of deactivating the catalyst. The cycles for the CeO_2 catalyst started to show both the discontinuity and the negative hysteresis as in the cycles without CeO_2 shown in Fig. 2b. This is consistent with the work of Fullerton, [15] who showed the presence of a small concentration of H_2S had the effect of significantly reducing the oxygen transfer capacity of CeO_2 which removed the benefits of having CeO_2 present.

For each of the studies with SO_2 the conversion of SO_2 to SO_3 was also calculated but this was not very repeatable. However, it was observed SO_2 competed with CH_4 for active sites, with CH_4 being more available. In contrast, when the conversion of SO_2–SO_3 started at the onset of PdO → Pd, there was a drop in methane conversion due to strong adsorption of SO_3. The conversion of SO_2–SO_3 increased to a maximum then decreased with temperature due to the thermodynamic instability of SO_3 [1]. This was also consistent with the work of Koutsopoulos et al. [16] which presented a similar study on powdered catalyst.

4.2. Methane oxidation in the absence, presence, and following SO_2 exposure

Fig. 6(a and b) shows the methane oxidation curves in the absence ('before'), presence ('with') and following ('after') SO_2 exposure for α of 0.2 for both catalysts. The equivalent graphs for α of 0.25 were plotted but are not shown due to the similarities with α of 0.2 in the trends obtained. For both catalysts it was found after exposure to SO_2 both an inhibition and a promotion effect were observed. The inhibition effect was at low temperature for the first cycle only. This was attributed to PdO–SO_x species below 860 K as discussed earlier. The promotion effect observed above 850 K is unusual for the oxidation conditions of the present study. In previous work [17], the regeneration of both sulphur-poisoned Pd/Al_2O_3 and Pd/CeO_2/Al_2O_3 catalyst was only partial under lean conditions of methane oxidation at temperatures 1023–1073 K, where our promotion effect was observed. In the previous work [17], alternate lean combustion/CH_4-reducing pulses experiments achieved a complete regeneration attributed to the decomposition of stable support sulphates. The presence of CeO_2 was found to partially hinder PdO sulphation.

The inhibition effect was successfully avoided in the present study by cutting the supply of SO_2 at 860 K. However, the promotional effect was not avoided by doing this (not shown). This implies the promotional effect was a result of a high temperature process with SO_2 when metallic Pd was likely to be present. For the Al_2O_3 supported catalyst, this promotional effect happened at the transition temperature range of PdO to Pd, and was short-lived. But

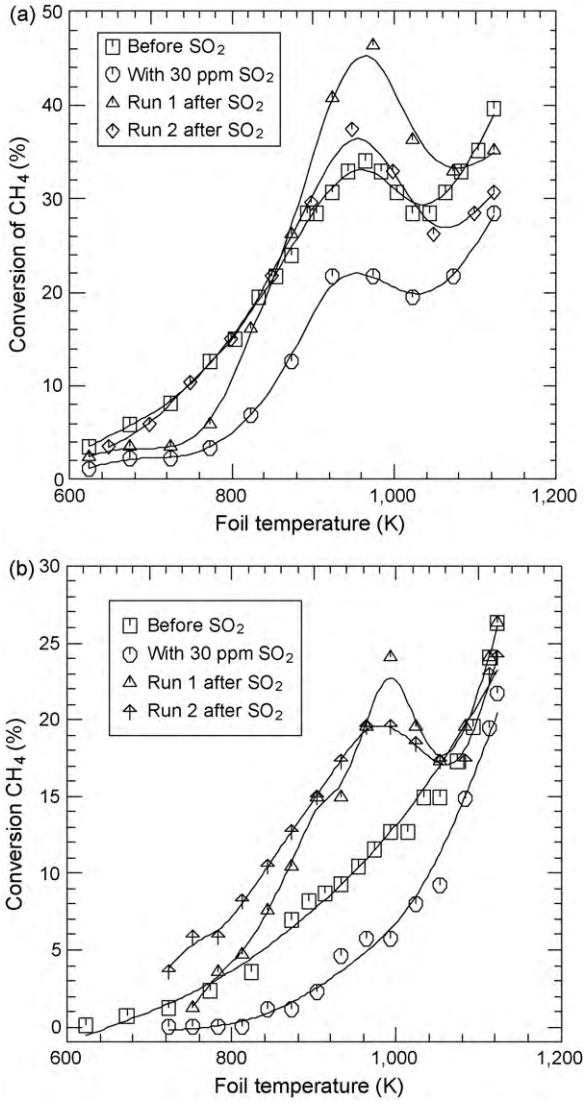

Fig. 6. Methane conversion in the absence, presence and following exposure to 30 ppm SO_2 doping (termed 'before', 'with', and 'after' in the legend respectively), increasing temperature with α = 0.2. (a) 3 wt.% Pd/γ-Al_2O_3. (b) 3 wt.% Pd/12 wt.% CeO_2/γ-Al_2O_3.

when CeO_2 was present, the promotional effect was more durable. One explanation is that the CeO_2 formed a sulphate during the exposure to SO_2, and this sulphate was slowly reduced back to CeO_2 by CH_4 in the following cycles. This would have provided a small release of SO_2.

In the work of Mowery and McCormick [11] there was evidence to suggest when PdO was reduced by SO_2, metallic Pd was formed in the core of PdO particles due to diffusion of oxide ions from the core. They presented a four step reaction step mechanism for this. When the PdO particle was exposed to SO_2 it was reduced to Pd, forming SO_3. The SO_3 then reacted with PdO to form $PdSO_4$ on the surface. The re-oxidation of surface Pd could then occur via two different ways, by oxygen from the gas phase or by diffusion of oxide ions from the interior. The latter would give rise to metallic Pd in the core. It was also suggested [11] a layer of $PdSO_4$ at the surface would restrict gas phase re-oxidation of Pd favouring the former mechanism. The formation of a metallic core would make the particles smaller. An alternative mechanism explaining such a promotion effect has been presented in [18] where Pt sulphation enhanced propane adsorption and such a process might facilitate methane adsorption and result in an increased activity with Pd.

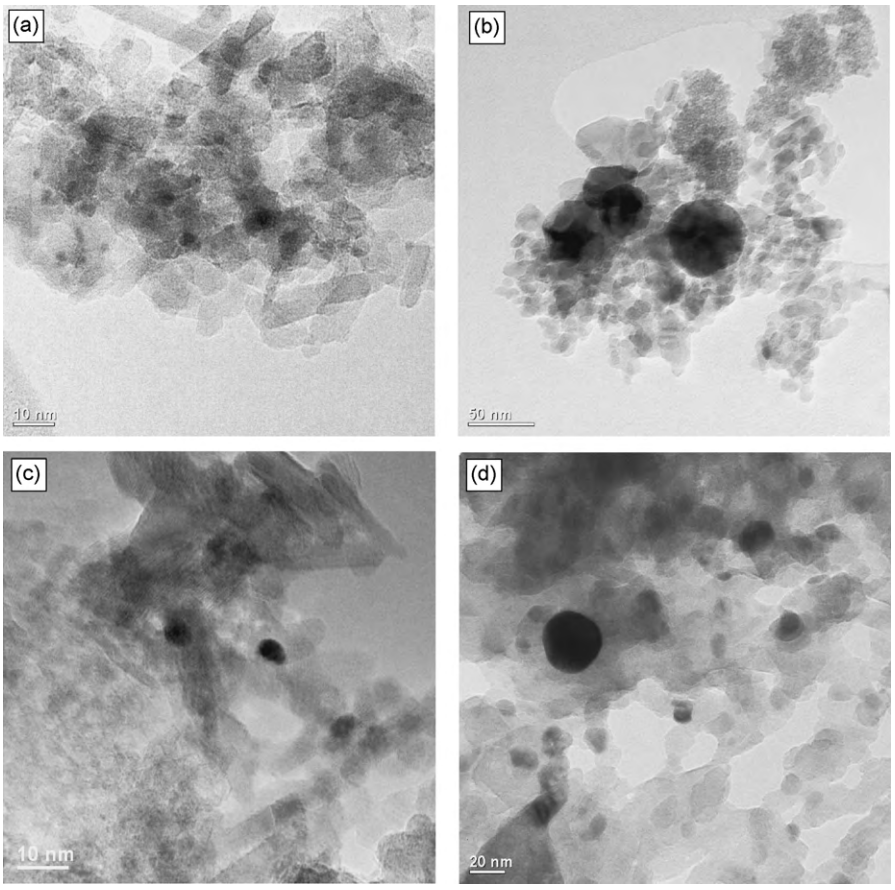

Fig. 7. TEM images before and after experiments. (a) Fresh (calcined) 3 wt.% Pd/γ-Al_2O_3, (b) Aged 3 wt.% Pd/γ-Al_2O_3, (c) Fresh (calcined)3 wt.% Pd/12 wt.% CeO_2/γ-Al_2O_3, (d) Aged 3 wt.% Pd/12 wt.% CeO_2/γ-Al_2O_3.

Before and after the experimental cycles the two catalysts were examined by TEM. Fig. 7 (a–d) show typical TEM images obtained for the fresh and aged catalyst respectively.

Comparing the metal (dark) particles in Fig. 7b with Fig. 7d, representative of 52 and 86 similar particle sizes obtained from TEM images for the aged Al_2O_3 and the aged CeO_2/Al_2O_3 washcoats respectively, revealed that on average the sizes of the PdO/Pd particles where 28% smaller in the ceria containing aged catalyst than the ceria-free aged catalyst. This was in spite of the ceria-containing having operated for 56% longer. The second point of interest was that the average size standard deviation for the CeO_2 containing catalyst was significantly lower. It can be concluded that the presence of CeO_2 significantly reduced sintering of the noble metal particles on the catalyst. Despite the differences in the Pt and Pd chemistries, this is consistent with previous studies [19] where platinum catalysts were investigated using the same reactor.

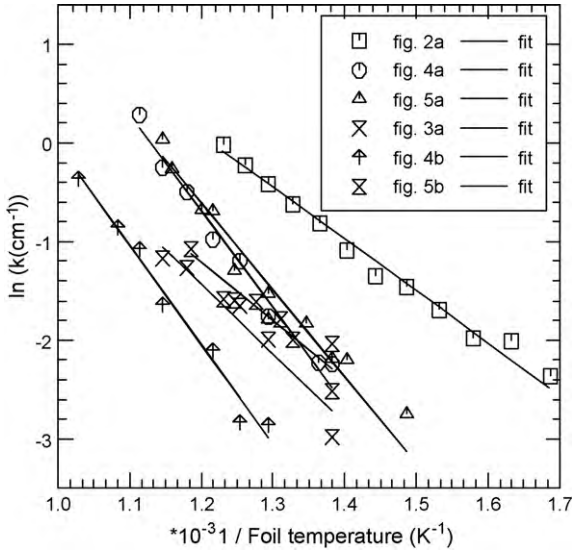

Fig. 8. Fits of linear regression of Eq. (1). The legend shows the figures in which the values of *A* and *E* were then used in SPIN to generate the conversion versus temperature model curves. All of the data points in the fits have an effectiveness factor in excess of 0.9 and belonged to the heating up part of the experiment.

Fig. 8 shows the linear fits obtained for the experimental conversion versus temperature curves using the methodology outlined in [3] and conversions below the PdO-Pd decomposition temperature. Table 1 displays the kinetic parameters that were derived from them. The values of *A* and *E* were then input into a one-reaction mechanism of methane oxidation in SPIN, together with the experimental temperature profiles and inlet conditions to generate the model curves shown in Figs. 2–5 alongside the experimental scatter points. It can be seen from the good linear fits of Fig. 8 and the modelled curves in Figs. 2–5 that the model and experimental kinetic data agreed well below the temperature of PdO decomposition.

5. Conclusions

Oxidation of CH_4 in the SPFR produced excellent repeatable results between temperature cycles for both for the Pd/Al_2O_3 and the $Pd/CeO_2/Al_2O_3$ catalysts in conditions prior to, during

and following SO_2 exposure The kinetic parameters derived in the lower temperature range below the PdO–Pd decomposition temperature together with a one-step chemical mechanism reproduced well the experimental conversion curves using SPIN. The discontinuity and hysteresis in methane conversion was attributed to the PdO–Pd conversions. The presence of CeO_2 was found to (i) stabilise PdO, effectively eliminating the discontinuity in the experiments with increasing temperature and (ii) reduce the sintering of the noble metal particles upon aging of the catalyst. However, the ceria containing catalyst had lower activity for methane oxidation. Exposure of the CeO_2-doped washcoat to 30 ppm SO_2 in the re-introduced the discontinuity in the methane conversion during the PdO–Pd conversion, thereby eliminating the observed stabilisation effect observed prior to exposure. A repeatable promotional effect on the methane conversion was observed following SO_2 exposure on both the Pd/Al_2O_3 and the $Pd/CeO_2/Al_2O_3$ washcoats. This may be attributed to the formation of a metallic core giving rise to reduction of PdO and creating more accessible active sites.

Acknowledgements

The authors would like to thank the EPSRC for a DTA award to GLR, Nagi Insura, and Johnson Matthey for catalysts and expertise.

References

[1] G.L. Rickett, Ph.D. thesis, University of Leeds, 2007. The Performance of Supported Noble Metal Catalysts in Conditions of Catalytic Combustion.
[2] M.E. Coltrin, R.J. Kee, G.H. Evans, E. Meeks, F.M. Rupley, F.J. Grcar, SPIN (version 3.83): A Fortran Program for Modeling One-Dimensional Rotating-Disk/Stagnation-Flow Chemical Vapor Deposition Reactor, Sandia National Laboratories Report No. SAND91-8003.UC 401, 1991.
[3] V. Dupont, J.M. Jones, S.-H. Zhang, A. Westwood, M.V. Twigg, Chem. Eng. Sci. 59 (2004) 17–29.
[4] R.E. Hayes, S.T. Kolaczkowski, Introduction to Catalytic Combustion, Gordon and Breach Science Publisher, Amsterdam, 1997.
[5] S. Lowell, J.E. Shieds, Powder Surface Area and Porosity, 2nd ed., Chapman and Hall, London, 1984, Chapters 8 and 9.
[6] T.R. Baldwin, R. Burch, Appl. Catal. 66 (1990) 337–358.
[7] O. Kubaschewski, C.B. Alcock, Metallurgical Thermochemistry, 5th ed., Pergamon, New York, 1979.
[8] G. Zhu, J. Han, D.Y. Zemlyanov, H.F. Ribeiro, J. Phys. Chem. B. 109 (2005) (2005) 2331–2337.
[9] A. Datye, J. Bravo, T.R. Nelso, P. Atannasova, M. Lyubovsky, L. Pfefferle, Appl. Catal. Gen. 198 (2000) 179–196.
[10] R.J. Farrauto, M.C. Hodson, T. Kennelly, E.M. Wasterman, Appl. Catal. Gen. 81 (2) (1992) 227–237.
[11] D.L. Mowery, R.L. McCormick, Appl. Catal. B. Environ. 34 (2001) 287–297.
[12] C.T. Campbell, D.C. Foyt, J.M. White, J. Phys. Chem. 81 (1977) 491–494.
[13] S. Colussi, A. Trovarelli, G. Groppi, J. Llorca, Catal. Comm. 8 (2007) 1263–1266.
[14] J.A. Lampert, M.S. Kazi, R.J. Farrauto, Appl. Catal. B. Environ. 14 (1997) 211–223.
[15] D.J. Fullerton, A. Westwood, R. Brydson, M.V. Twigg, J.M. Jones, Catal. Today 81 (4) (2003) 659–671.
[16] S. Koutsopoulos, S.B. Rasmussen, K.M. Eriksen, R. Fehrmann, Appl. Catal. 306 (2006) 142–148.
[17] F. Arosio, S. Colussi, G. Groppi, A. Trovarelli, Top. Catal. 42–43 (2007) 405–408.
[18] R. Burch, E. Halpin, M. Hayes, K. Ruth, J.A. Sullivan, Appl. Catal. B. Environ. 19 (1998) (1998) 199–207.
[19] G. Rickett, V. Dupont, M.V. Twigg, J. Energ. Inst. 76 (7) (2006) 12–18.